Ultra-high areal capacitance and high rate capability RuO2 thin film electrodes for 3D micro-supercapacitors

Bouchra Asbani, Gaëtan Buvat, Jeremy Freixas, Marielle Huvé, David Troadec, Pascal Roussel, Thierry Brousse, Christophe Lethien

HAL Id: hal-03395314
https://hal.science/hal-03395314

Submitted on 25 May 2023

Ultra-high areal capacitance and high rate capability RuO₂ thin film electrodes for 3D micro-supercapacitors

Bouchra Asbani[1,2], Gaetan Buvat[1,2], Jeremy Freixas[1,2,3], Marielle Huvé[4], David Troadec[1], Pascal Roussel[4], Thierry Brousse[2,3*] and Christophe Lethien[1,2,5*]

[1] Université de Lille, CNRS, Centrale Lille, Université Polytechnique Hauts-de-France, UMR 8520 - IEMN, F-59000 Lille, France

[2] Réseau sur le Stockage Electrochimique de l'Energie (RS2E), CNRS FR 3459, 33 rue Saint Leu, 80039 Amiens Cedex, France

[3] Institut des Matériaux Jean Rouxel (IMN), CNRS UMR 6502 – Université de Nantes, 2 rue de la Houssinière BP32229, 44322 Nantes cedex 3, France

[4] Unité de Catalyse et de Chimie du Solide (UCCS), Université de Lille, CNRS, Centrale Lille, Université d'Artois, UMR 8181 – UCCS, F-59000 Lille, France

[5] Institut Universitaire de France (IUF)

*Correspondence to: christophe.lethien@univ-lille.fr & thierry.brousse@univ-nantes.fr

ACKNOWLEDGEMENT

MATERIALS & CORRESPONDENCE

Correspondence to Christophe Lethien & Thierry Brousse

Ultra-high areal capacitance and high rate capability RuO$_2$ thin film electrodes for 3D micro-supercapacitors

KEYWORDS: RuO$_2$, thin films, pseudocapacitance, 3D micro-supercapacitor, rate capability

ABSTRACT: To power the next generation of miniaturized electronic devices, 3D micro-supercapacitors are a new class of millimeter scale electrochemical capacitors with superior storage performance than their planar counterparts. Nevertheless, it is mandatory to carefully match the dimensions of the 3D scaffold with the thickness of the electrochemically active electrode materials to take benefit from both the high capacitance values and the high rate capability of 3D micro-supercapacitors technology. Here we demonstrate how to design an efficient 3D electrode based on ruthenium oxide pseudocapacitive film (~400 nm-thick) deposited on a robust 3D scaffold. ~90% of the initial capacitance value is maintained during 10000 cycles. The proposed 3D RuO_2 electrode exhibits remarkable areal capacitance values (~4.5 Fcm^{-2}) at 2 mVs^{-1}, while maintaining more than 2 Fcm^{-2} at 100 mVs^{-1} (10 s charge / discharge time), thus validating the design of ultra-high capacitance electrode with high rate capability.

INTRODUCTION

Over the last decade, the miniaturization of electrochemical capacitors' technology[1–3] has triggered a great interest for powering miniaturized electronics and wearable devices[4,5]. A micro-supercapacitor (MSC) is a class of miniaturized electrochemical capacitor[2,3] integrated on a flexible or a rigid substrate - ideally a silicon wafer to be compatible with semiconductor industry - and showing low footprint surface, high rate capability and long cycle life[1,6–10]. While such micro-devices are able to sustain high peak current, the main challenge consists in improving the energy density and so maximizing the amount of active material in the electrodes. As the footprint area is a critical issue for such miniaturized electronics, the *areal* capacitance, power and energy densities are the most suitable metrics used to define the guidelines for optimizing micro-supercapacitors[11,12].

As mentioned in a recent review[4], two strategies can be followed to maximize the areal energy density of micro-supercapacitors operating in aqueous (~1 V) and organic electrolytes (~3 V). A first approach consists in tuning the thickness of the capacitive electrode, whatever the implemented electroactive materials (i.e., porous carbon or pseudocapacitive materials). In that case, it is important to distinguish the thin and the thick films technologies and an arbitrary limit has to be fixed for discussion. For micro-supercapacitor applications, the deposition method of the active material has to be compatible with mass production to favor a rapid scale-up of the technology[1,8]. Among the existing deposition methods widely used in the semiconductor industry, Physical Vapor Deposition (PVD) technique is an interesting solution: deposition of 5 µm-thick film on silicon substrate or III-V substrate is easily achieved using such technique. Thus, we arbitrarily decided to set the limit close to 5 µm to distinguish the thin and thick film approaches. While the thin film technology is

recognized to be a powerful approach from scaling-up and rate capability optimization, the areal energy density of the proposed technology is still limited. On the other side, thick film technology allows producing high areal capacitance value, but with limited rate capabilities if a careful material design (i.e., mixing of active material with conducting agent) is not achieved within the electrode, that is to say a tuning of the film morphology to favor rapid ion diffusion and fast electron transport[13–16]. In that case, it is quite complicated to produce a large number of micro-devices per substrate (mass production) because the deposition methods of those thick composite electrodes is not fully compatible with collective fabrication technique, i.e. it is limited by the resolution of deposition techniques, usually in the order of tens of micrometers.

Taking into account the restricted footprint surface of the micro-supercapacitor, the mass-production compatible deposition method and the limited thickness of the active material (rate performance), an attractive way consists in designing 3D electrodes with large surface to volume ratio to maximize the interaction between the active material and the electrolyte. Since the last five years, a 3D paradigm shift occurs for designing efficient micro-supercapacitors[4,7,17–19] following the same technological roadmap than the lithium-ion micro-batteries technology[20–22]. The capacitance of the 3D MSC is thus improved by up to two order of magnitude as compared to the planar topology. In this context, powering the next generation of Internet of Things (IoT), wearable electronics or wireless sensor network technologies (all these technologies requiring miniaturized power sources with remarkable energy density, high rate capabilities and long cycling life) becomes feasible.

The fabrication of 3D micro-supercapacitors with outstanding energy density requires the manufacturing of robust and efficient 3D scaffold. Top down and bottom up synthesis techniques are widely used to produce self-organized 3D nano- or micro-structures[7,17,18,23–25] with specific surface. In that case, the conformal deposition of active material (MnO_2, RuO_2…) on those 3D scaffolds allows maximizing the areal capacitance value.

Herein we demonstrate the production of 3D electrodes with ultra-high capacitance values. Our approach consists in combining an efficient and robust 3D scaffold with RuO_2 pseudocapacitive thin films allowing maximizing the areal capacitance without any degradation of the rate performance. We show that it is possible to reach a remarkable areal capacitance value ($\sim$ 4.5 Fcm^{-2} at 2 mVs^{-1}) with only $\sim$ 400 nm-thick RuO_2 film. More impressively, the combination of highly efficient 3D scaffold together with RuO_2 thin film allows delivering $\sim$ 2 Fcm^{-2} at 0.1 Vs^{-1} (charging time $\sim$10 s), thus validating the high rate performance of the 3D electrode. This record capacitance is among the highest reported values in the last 10 years in that field. Our approach emphasizes the importance to carefully match the dimension of the 3D scaffold with the thickness of the active material.

RESULTS AND DISCUSSION

The general strategy used in the frame of this study to maximize the performance of 3D micro-supercapacitors is reported in **Fig. 1.** We propose to maximize the areal capacitance values of electrodes of micro-supercapacitors while keeping high the rate capability. To reach this goal, an attractive solution consists in depositing a thin film of active material on 3D scaffold while keeping constant the footprint area of the electrodes. To maximize both the areal capacitance values and the rate capability, two critical parameters have to be tuned, corresponding to the *x* and *y*-axis of the **Fig. 1a**. It is well known that the performance of 3D electrodes are evaluated regarding the area enhancement factor of a template (AEF, *y*-axis of the **Fig. 1a**), representing the ratio between the 3D surface to the footprint surface (3D/2D ratio). To optimize the performance of the 3D micro-supercapacitor, it is crucial to be able to predict the Area Enlargement Factor (AEF) of the 3D scaffold based, in this specific study, on vertically aligned silicon micro-tubes. The active material (here, the RuO_2 thin film) of the MSC has to be deposited by step-conformal deposition method on 3D scaffold showing a large specific surface (S_{3D}) while maintaining constant the surface footprint (S_{planar}). Indeed, the miniaturization of electrochemical capacitor technology impose the use of small footprint surface. The AEF could be mathematically defined as the ratio between the real surface area (S_{3D}) developed by the 3D electrode on the footprint surface (S_{planar}). Regarding the shape of the proposed scaffold, the diameters of the structural features and the spacing between two micro-tubes were tuned to fulfil the technological and performance requirements. From a mathematical point of view, the AEF of the 3D micro-tube topology is given by: $AEF = \dfrac{S_{3D}}{S_{planar}} = 1 +$

$\dfrac{(P_{IN} \times d_{IN} + P_{OUT} \times d_{OUT})}{pitch^2}$

where pitch is the structure pitch (the sum of the outer diameter (OD) of a single micro-tube and the spacing between two micro-tubes); p_{out} and p_{in} are the outer and inner perimeters, respectively, at the micro-tube base; and d_{out} and d_{in} are the outer and inner depth, respectively, of the micro-tubes. ID refers to the inner diameter of a micro-tube. More information could be found in the experimental section. Taking into account the AEF (**Fig. S1a**), the capacitance of a 3D MSC could be clearly enhanced as compared to the one of planar MSC according to the formula: C_{3D} (Fcm^{-2}) = AEF x C_{planar} = S_{3D} / S_{planar} x C_{planar}

Moreover, the areal capacitance value of an electrode is maximized by improving the amount of active material, *i.e.* the thickness of the electrode (x-axis of the **Fig. 1a**). Here we propose to tune both the AEF of a 3D scaffold based on a silicon micro-tubes array[22,26] and the thickness of hydrous ruthenium oxide films[27,28] to maximize the performance. To avoid multiplying the possible parameters to be varied, we kept constant the inner and outer diameters of the silicon micro-tubes as well as the structure pitch of the 3D scaffold. Thus, to modify the AEF value, we just need to tune the depth (from 45 up to 150 µm) of the 3D micro-tubes, as proposed in **Fig. 1b** corresponding to AEF values ranging from 18 to 56, respectively. On the other hand, we also tuned the amount of active material through the control of the RuO_2 films thickness, from 100 nm up to 436 nm as depicted in **Fig. 1c**. We thus evaluated the electrochemical performance of 3D electrodes according to these two critical parameters.

Numerous 3D electrodes were fabricated as follows. In a first step, the 3D silicon micro-tubes were fabricated using a Deep Reactive Ion Etching (DRIE) Bosch process[4,7], ensuring a good tradeoff between robustness, enhancement of the active area and dense 3D silicon micro-tubes. The micro-tubes were then protected

by an insulating layer of Si_3N_4 using LP CVD (or alternatively, with an Al_2O_3 layer made by ALD, see method section). A film of Pt (~50 nm), acting as a current collector, was deposited using atomic layer deposition (ALD) method. Finally, a hydrous RuO_2 thin film was electrodeposited on the resulting 3D conducting architecture. More experimental details can be found in the experimental section and the recent published work by our group[7,17]. To deposit a conformal RuO_2 film, only the sweep rate of the CV of the electrodeposition process was tuned (**Fig. S1a**). **Figure S1b** describes the evolution of the film thickness, measured at the top and the bottom of the tubes, at different sweep rates from 10 to 50 mVs^{-1}. The amount of active material and the conformal deposition of the ruthenium dioxide films are directly proportional to the thickness of the diffusion layer in the cyclic voltammetry deposition experiment. The thickness of the diffusion layer (δ) is given by the following equation

$\delta = \sqrt{\dfrac{DRT}{Fv}}$ where D is the diffusion coefficient, R is the gas constant, T is the temperature, F is the Faraday constant and v is the sweep rate of the CV experiments. From this equation, it can be deduced that the thickness of the diffusion layer is high at low scan rate. On the other hand, high scan rate values lead to thinner diffusion layer. Consequently, a large amount of active material (i.e. thickness RuO_2 ~ 400 nm) stays at the top of the 3D micro-tubes when the sweep rate of the CV is low (ex: at 10 mV.s^{-1}) because the thickness of the diffusion layer is large, i.e. in the same order of magnitude of the inner diameter of a micro-tube and the spacing between two micro-tubes. At higher sweep rate (ex: at 50 mV.s^{-1}), the diffusion layer is nanometer-thick thus reducing the amount of deposited active material (i.e. RuO_2 ~ 100 nm-thick) while allowing a good conformal deposition from the top to the bottom

of the micro-tube scaffold. In summary, at low sweep rate, the electrodeposited RuO_2 film was not homogeneously deposited all along the depth of the micro-tubes. On the other hand, the RuO_2 film thickness was uniform from the top to the bottom of the 3D micro-tubes scaffold when the sweep rate reaches 50 mVs^{-1}. SEM top views and cross-sections analyses confirmed the conformal deposition of the RuO_2 film from the top to the bottom of 3D micro-tube (**Fig. S1c**). Based on these optimizations, the deposition of RuO_2 pseudocapacitive films was hereafter achieved by cyclic voltamperometry in $RuCl_3$/HCl/KCl solution at 50 mVs^{-1} and 50 °C. The evolution of the RuO_2 thickness vs the number of electrodeposition cycles was proposed in **Fig. S1d**. The hydrous form of ruthenium oxide was confirmed by Raman spectroscopy and depicted in **Fig. S1e**.

(S)TEM and EDS analyses were performed to study the interfaces between all the deposited layers of the 3D electrodes. The HAADF image of a FIB lamella (**Fig. 2a and Fig. S2a**) as well as the EDS chemical mapping (**Fig. 2 a$_1$ to a$_6$**) confirmed the perfect deposition of the stacked Al_2O_3 / Pt / $hRuO_2$ layers on the Si micro-tube scaffold (**Fig. S2a**). Note that the presence of Si element, which was expected in the center of the tube, (**Fig. 1**), was not detected by EDS because the FIB lamella was too thin (~150 nm-thick) to reveal the deep layers. The thicknesses of the $hRuO_2$ / Pt / Al_2O_3 stacked layers were approximately close to 85 nm, 75 nm, 40 nm (**Fig. 2b**), respectively, according to the EDS chemical mapping (**Fig. S2**). The homogeneity of the layers was confirmed by the EDS results (**Fig. 2 a$_1$ to a$_6$ and Fig. S2b**) with a small diffusion of Pt in hydrous RuO_2 ($hRuO_2$). It can be noted that a large part (yellow color) of Pt observed in **Fig. 2a$_1$ and a$_3$** came from the FIB preparation with redeposit of the protected Pt layer issued from the FIB preparation (see methods section). The HRTEM images of the different interfaces (**Fig. 2c and S3**) reveal

crystalline nanodomains for each layers. The inter-fringe distance of 2 Å corresponds to the inter-planar spacing d_{200} of the Pt, while, as already observed in ref [29], the inter-planar spacing of 2.2 Å could be assigned to the d_{111} of the rutile-like phase constituting the hydrous RuO_2 nanodomains.

The kinetic limitations (ion diffusion, electron transport) of the 3D RuO_2 electrodes were first evaluated regarding the thickness of the active films (from 100 up to 436 nm), while keeping constant the surface to volume ratio of the 3D scaffold (here, the AEF was set to ~40 according to the depth of the Si micro-tubes template (100 µm)). The cross-section images of four 3D electrodes (**Fig. 1c)** confirm the presence of a conformal RuO_2 deposit all over the depth of 3D silicon micro-tube. The reproducibility of our fabrication process allowed us to further investigate the electrochemical behavior of the 3D RuO_2 electrodes. Their capacitance were determined using cyclic voltammetry in 0.5 M H_2SO_4. Electrochemical performance are summarized in **Fig. 3 and S4**. The CV shapes of the four 3D RuO_2 electrodes measured at 2 mV s^{-1} correspond to that of RuO_2 pseudocapacitive material as previously shown[30–32]. The CVs at different sweep rates are reported in **Fig. S4a-d**. Indeed, the change in the oxidation state of the ruthenium cations is balanced by the surface/near surface insertion-desinsertion of protons coming from the H_2SO_4 aqueous electrolyte[30–32]. The CV plots exhibit two sets of redox reaction peaks (~0.2 V and 0.45 V vs Ag/AgCl) with a good symmetric shape during forward and backward scans. Moreover, we observed a significant improvement of the CV intensity resulting from the increasing thickness of active material. The variation of areal capacitance was extracted from CVs at 2, 25 and 50 mVs^{-1} and reported in **Fig. 3b and S4e** *vs* the of RuO_2 thickness**.** Notably, at 2 mVs^{-1}, the areal capacitance - C_s - continuously improves from 0.4 to 2.8 Fcm^{-2} when the thickness increases from 100

to 436 nm (**Fig. 3b**). The corresponding volumetric capacitance (C_v) value of the active material is then ~ 1400 Fcm^{-3} (**blue curve - Fig. 3b**), in the range of vanadium nitride and MXene pseudocapacitive materials[8,14]. This volumetric capacitance was calculated according to the whole volume of deposited RuO_2 films which takes into account the AEF of the 3D scaffold substrate, i.e. $C_v = C_s$ / (AEF x thickness). More interestingly, the capacitance value of 436 nm-thick RuO_2 electrode is maintained at 1.6 Fcm^{-2} (**Fig. S4e**) for higher sweep rate (50 mVs^{-1}) and the b-coefficient (**Fig. 3c and S4f**), extracted from the power law $I_{peak} = av^b$ (where a and b are parameters related to the electrode), stayed in the range of 0.90 ± 0.05 whatever the thickness. This confirms that charge storage process is not limited by the ion diffusion within the 3D electrodes, for such RuO_2 film below 500 nm thickness. The kinetic limitation of the 3D electrodes was more accurately investigated using electrochemical impedance spectroscopy (**Fig. 3d**). The Nyquist plots are in agreement with that of pseudocapacitive materials with a semi-circle behavior at high frequency showing the charge transfer process and a quasi-vertical line at low frequency. From the impedance spectra, we extracted the evolution of the equivalent series resistances for each RuO_2 thickness (**Fig. 3d - inset**). This evidences a weak increase of the ESR (from 1.3 to 2.1 $ohm.cm^2$) with the thickness. Indeed, as the amount of deposited RuO_2 increases it becomes more difficult to quickly access to the whole electroactive surface and subsurface.

Finally, we evaluated the stability performance (**fig. 3e**) of two 3D RuO_2 electrodes (AEF > 40, RuO_2 thickness > 250 nm) in 0.5M H_2SO_4 upon cycling. On one hand, the as-deposited 3D RuO_2 electrode clearly shows a significant decrease of the capacitance retention, where only 60 % of the initial capacitance value is maintained after 8 000 cycles while the coulombic efficiency stays close to ~ 100 %. On the other

hand, the air-annealed 3D RuO$_2$ electrode (150 °C during 1h) shows much improved cycling performance with 86 % of the initial capacitance retains after 10 000 cycles. Thus, the air annealing process allows stabilizing the cycling performance of the 3D RuO$_2$ electrode tested in 0.5M H$_2$SO$_4$ aqueous electrolyte.

In this first part, we shown that, for constant AEF value of 40, rate performance of the 3D RuO$_2$ film is not strongly limited for active material thicknesses below 500 nm. Nevertheless, it is also very important to clarify how the design of the 3D scaffold influences the electrochemical performance of the 3D RuO$_2$ electrodes. To reach this goal, we modified the depth of the 3D silicon micro-tubes to vary the AEF values from 15 (38 µm-depth) to 66 (170 µm-depth). As previously mentioned, the inner and outer diameters as well as the pitch of the 3D microstructures were not modified. 200 nm-thick RuO$_2$ films were then deposited on the corresponding 3D scaffold following the same deposition process used in the previous part of this paper. The electrochemical performance of the 3D RuO$_2$ electrode regarding various AEF values (AEF = 15, 23, 30, 40, 54, 66, respectively) are reported in **Fig. 4, S5 and S6**. The CV plots measured at 2 mVs^{-1} are presented in **Fig. 4a**, while the CVs at other sweep rates are shown in **Fig. S5.** From these plots, we clearly demonstrate the strong influence of the AEF factor onto the areal capacitance (**Fig. S6a**). From those CVs, the evolution of the areal capacitance at various sweep rates was then plotted regarding the AEF factors (**Fig 4b**). Note that volumetric capacitance was not evaluated in the present case because it only depends on the thickness of active material and in no case from the AEF value. At 2 mVs^{-1}, the areal capacitance of the 3D electrodes (200 nm-thick) is enhanced from ~ 0.12 Fcm^{-2} to ~ 3 Fcm^{-2}. More importantly, 66% of this high capacitance (~ 2 Fcm^{-2}) value is kept at high sweep rate (100 mV.s^{-1}) validating

the high rate capability of our 3D RuO$_2$ electrodes. The shape of the impedance spectra (**Fig. 4c**) is similar to that reported in **Fig. 3**. From theses Nyquist plots, we evaluated the evolution of the ESR value *vs* the AEF factor for 200 nm-thick RuO$_2$ films (**Fig. 4d**). We observe an increase of the ESR value from 1 to ~3.5 ohm.cm^2 when AEF varies from 15 up to 66. While the areal capacitance values were remarkably improved with the 3D technologies, we show that deep 3D scaffold does not induce strong kinetic limitations, allowing high rate performance of the 3D electrodes. This conclusion is further validated by the results reported in **Fig. S6** where the kinetic limitations is studied from the CVs curves. From the evolution of I$_{peak}$ *vs* the sweep rate (**Fig. S6b**), we can deduce the variation of the b-coefficient *vs* the AEF: the b value stays close to 0.95 ± 0.05 whatever the AEF (**Fig. S6c**).

This remarkable performance in term of areal capacitance values and rate capabilities of the 3D RuO$_2$ electrode is attributed to their tailored design:

(i)   the geometric dimensions of the 3D scaffold were optimized to produce a robust template with high specific area (i.e., high AEF values).

(ii)   the thickness of the pseudocapacitive RuO$_2$ film was willingly limited (< 500 nm).

(iii)   the electrodeposition process was optimized to produce conformal deposits which enabled to avoid deposition of RuO$_2$ material localized only at the top of the 3D structures as it is sometimes observed.

The fine-tuning of the 3D electrode allowed facilitating the ion diffusion and the transport of electrons, providing abundant active sites for charge–transfer reactions between the active materials and the liquid electrolyte, thus ensuring a larger utilization of RuO$_2$ electroactive material. Some recent papers[18,19,33,34] showed high capacitance values, but exhibited low rate performance, which in turn limits the

power density of the related microdevices. To investigate the kinetic limitation of the 3D RuO_2 electrodes, we applied a data processing method earlier proposed by Trasatti and co-workers for thin film electrodes[28]. **Fig. S6d-f** shows the sweep rate dependence of q^* and $1/q^*$ according to the AEF values, where q^* are the charges related to the "inner" (less accessible active surface) and the "outer" (more accessible active surface), respectively. From these q^* data investigation, the outer capacity ($q_{surface}$) and the total one (q_{total}) are calculated and plotted versus the AEF factor, taking constant the thickness (200 nm) of RuO_2 films (**Fig. S5f**). The $q_{surface}$ and q_{total} values reach 1.4 and 3.2 Fcm^{-2}, respectively, demonstrating again the high areal capacitance and rate capability of our 3D RuO_2 electrodes.

Taking advantages of tuning both the AEF and the RuO_2 thickness, an ultra-high performance 3D electrode was prepared and the results are summarized in **Figure 5**. 170 µm-depth silicon micro-tubes scaffold (AEF = 66) was coated with 427 nm-thick RuO_2 films (**Fig. 5a**). The electrochemical performance were then evaluated in 0.5M H_2SO_4. The CV (green plot) at 2 mV s^{-1} is reported in **Fig. 5b** and compared with the CV of a 3D electrode showing the same AEF value but coated with only 200 nm-thick RuO_2 film (pink plot). The CVs at other sweep rates are depicted in **Fig. S7a-b**. The CV profiles correspond again to that previously reported for electrodeposited RuO_2 tested in aqueous electrolyte. Not surprisingly, the CV area of the 427 nm-thick 3D electrode is larger than the 200 nm-thick one, meaning that the surface capacitance value is maximized owing to the larger amount of pseudocapacitive RuO_2 material in thicker electrodes. In **Fig. 5c**, the areal capacitance values of the two 3D electrodes are plotted *vs* the sweep rates, from 2 up to 100 mVs^{-1}. At the lowest scan rate (i.e. at 2 mVs^{-1}), the areal capacitance of the 427 nm-thick 3D electrode is approximately 4.3 Fcm^{-2} while the corresponding capacitance value for the 200 nm-thick 3D electrode is

~ 3 Fcm^{-2}. When the sweep rates is higher than 20 mVs^{-1}, the pink and green plots converge to the same value meaning that some kinetic limitations occurred with the thicker layer at high scan rate. At 100 mVs^{-1} (10 s charging / discharging time), the two 3D electrodes were able to deliver more than 2 Fcm^{-2}. To investigate the kinetic limitations within the 3D electrodes, we used one more time the "Trasatti" data processing method[28] to extract q_{total} and $q_{surface}$ from the CV measurements. On one hand, the evolution of q* *vs* the inverse square root of the sweep rate was shown in **Fig. 5d**. At high sweep rate, that is to say at 1/v → 0 mVs^{-1}, the $q_{surface}$ values are 1.5 and 1.75 Ccm^{-2} for the 200 and 427 nm-thick 3D electrodes respectively. On the other hand, the evolution of 1/q* vs the square root of the sweep rate was shown in **Fig. 5e**. At low sweep rate (v → 0 mVs^{-1}), the $1/q_{total}$ values are 0.2 and 0.32 cm^{2}C^{-1} corresponding to q_{total} values of ~ 3.1 and 5 Ccm^{-2} respectively. Taking into account a 1V potential windows, these capacity values translate into 1.5 and 3.1 Fcm^{-2} for the 200 nm-thick 3D electrode and 1.75 and 5 Fcm^{-2} for the 427 nm-thick 3D electrode. The results are summarized in **Fig. 5f** where a comparison is made between the two electrodes. Interestingly, the areal capacitance value of the 200 nm-thick 3D electrode measured at 2 mVs^{-1} (blue bar) represents 96% of the total capacitance determined from Trasatti analysis. That is to say that most of the capacitance is delivered within 500 s discharge time. For the thicker 3D electrode, this value decreases down to 84 % of the total capacitance which is still a reasonable value for 500 s discharge time. Moreover, the capacitance value of the 427 nm 3D electrode at high sweep rate is quite remarkable (2 Fcm^{-2}), thus emphasizing the importance of carefully tuning the film thickness to maximize both areal capacitance and the rate capability. To illustrate this point, a benchmark of the surface capacitance as a function of the film thickness is reported in **Fig. 5g-i and Fig. S7c**. Clearly, the

technology developed in this study leads to very high capacitance values (~ 4.5 Fcm^{-2}) compared to literature data on 2D thin and thick film electrodes **(Fig. S7c)**. To improve the performance of MSCs' electrodes, it is commonly admitted that an increase of the film thickness allows maximizing the surface capacitance[4]. Nevertheless, even if this strategy is widely used for large scale electrochemical capacitors where active material is mixed with binders and conducting additives to boost the electrical conductivity, it will not be easily transferred to microscale devices where the electrodes are made from film deposition under vacuum or electrodeposition methods. In that case, no conducting agent is used to improve the electrical conductivity, meaning that kinetic limitations occurred when thicker layers are used. For a sake of clarity and as already proposed[4], we fixed a limitation between what we call thin and thick film technologies: in that case, 5 µm represents the threshold that we selected to dismiss the two technologies. For thin film electrodes (thickness < 5 µm, blue cross, **Fig. S7c**), the surface capacitance value does not exceed 0.5 Fcm^{-2}. For thick film electrodes (thickness > 5 µm, pink cross, **Fig. S7c**), the surface capacitance value does not exceed 1.5 Fcm^{-2}, even for more than 100 µm-thick films.

It is also important to benchmark our results regarding the existing 3D electrodes (**Fig. 5g-i**). Numerous papers were published the last five years regarding the fabrication of 3D micro-supercapacitors based on efficient and high performance electrodes. Carbon nanowalls[25], silicon nanowires[24,35,36], porous metallic templates[18,19,34], nickel nanorods[23] and silicon micro-pillars or micro-tubes[7,17] were used as efficient scaffolds to improve the surface area of small footprint electrodes. When those 3D scaffolds are decorated with capacitive or pseudocapacitive materials, the areal performance are significantly enhanced.

Nevertheless, it is mandatory to match carefully the design (AEF) of the 3D template with the amount (thickness) of deposited active material. On one hand, if the amount of active material and the AEF are too low, the overall performance of the 3D electrode will be weakened. On the other hand, if the electrode material is too thick and completely fills the 3D scaffold, the expected 3D effect will disappear and kinetic limitations will arise. In particular, for micro-supercapacitors with a time constant ~10 s, it makes no sense to maximize the areal capacitance at low charge/discharge rates with thick layers of active material if kinetic limitations occur when the MSC is to be solicited at higher rates in a practical use. The **Fig. 5g** reports on the benchmark of the existing 3D electrodes *vs* the thickness of active material and the results of the present study are implemented in the same plot. Interestingly, above 5 µm thickness, a larger increase in capacitance with deposited active material thickness is observed **(Fig. 5g)** as compared to the thinner layers. However, a detailed analysis of rate capability for the related thick films above 5 µm (**Fig. 5h and 5i**) reveals that this increase in capacitance goes together with a decrease in the rate capability of the related electrodes. Considering thin layer of active material (thickness < 5 µm) deposited on 3D scaffold, our 3D electrodes exhibit the highest areal capacitance (~4.5 Fcm^{-2}) values reported up to now. This value is four fold higher than the areal capacitance value reported for RuO_2 electrodes based on carbon nanowalls[25] and ten times higher than what we recently obtained with MnO_2 electrodes[7,17]. If we compare our results on thin layer (<0.5 µm) with data on thick ones[18,19,34] (thickness > 5 µm), the surface capacitance values of the proposed 3D electrodes are at the same level of magnitude, as shown in **fig. 5g**. Only the last results published by the group from D. Pech and D. Guay on 3D $RuO_xN_yS_z$ electrode[34] exhibit a higher capacitance value (~9.4 Fcm^{-2} at 2 mVs^{-1}). Nevertheless, it is

important to compare the performance of 3D electrodes for MSC both at low and fast charge / discharge sweep rates. Hence, we extracted the areal capacitance values measured at 2 mVs^{-1} (pink bars) and 100 mVs^{-1} (blue bars) of most of the 3D published within the literature (only the papers reporting an areal capacitance > 0.5 Fcm^{-2} were considered). The surface capacitances (in Fcm^{-2}) and the normalized capacitances (per µm of active material, in Fcm^{-2}µm^{-1}) *vs* the film thickness are summarized in **Fig. 5h-i**. As depicted in **Fig. 5h**, the 3D RuO$_2$ electrodes proposed here exhibit the best "C$_{surface}$ @ 2 mVs^{-1} / C$_{surface}$ @ 100 mVs^{-1}" compromise, thus validating the use of such electrodes for delivering ultra-high capacitance values at both high and low rate. 66% and 50% of the areal capacitance value measured at 2 mVs^{-1} are delivered at 100 mVs^{-1} for the 200 nm-thick and 427 nm-thick RuO$_2$ electrode, respectively. We also observe that, due to kinetic limitations, a large amount of material is electrochemically inactive when thick layer (> 5 µm) are used at high sweep rate[18,19,34]. By normalizing the surface capacitance of the electrode by the thickness of the active material, we observed again the superior behavior of the proposed 3D electrodes (**Fig. 5i**). We can conclude that the careful matching between the dimension of the 3D scaffold and the thickness of active material allows maximizing the general performance of the MSC electrodes with an optimal amount of electrochemically active RuO$_2$ material. The next actions will consist in the fabrication of 3D solid-state RuO$_2$/RuO$_2$ interdigitated MSC using microfabrication technique[6,7] widely developed in the semiconductor industry. Considering a cell voltage of 1 V and a cell capacitance of ~ 1 Fcm^{-2} (one fourth of the electrode capacitance if an interdigitated topology is considered[4,5]), the energy density of those MSCs should reach more than 0.14 mWhcm^{-2} while keeping power density in the range of 1 - 10 mWcm^{-2}. Hence, the performance of those MSCs will allow getting

autonomous small electronic devices particularly useful for the next generation of miniaturized IoT technology.

CONCLUSION

In summary, we demonstrated the fabrication of efficient 3D electrodes based on a robust 3D silicon-scaffold (AEF = 66) and the deposition of ~400 nm-thick RuO_2 films. At the lowest scan rate (2 mVs^{-1}), the areal capacitance of a 427 nm-thick 3D electrode reaches 4.3 Fcm^{-2} while at 100 mVs^{-1} (10 s charging / discharging time), the 3D electrode is still able to deliver more than 2 Fcm^{-2}. A ~90% retention of the initial capacitance was obtained over 10000 cycles. The fabrication of ultra-high capacitance 3D electrodes with high rate capabilities was demonstrated in this study thus emphasizing how much is important the matching the dimension of the 3D scaffold with the thickness of the electrochemically active electrode materials.

DATA AVALAIBILITY

The raw/processed data required to reproduce these findings cannot be shared at this time as the data also forms part of an ongoing study.

COMPETING INTERESTS

The authors declare no competing interests.

MATERIALS & CORRESPONDENCE

-

REFERENCES

[1]   P. Huang, C. Lethien, S. Pinaud, K. Brousse, R. Laloo, V. Turq, M. Respaud, A. Demortière, B. Daffos, P.L. Taberna, B. Chaudret, Y. Gogotsi, P. Simon, On-chip and freestanding elastic carbon films for micro-supercapacitors, Science (80-.). 351 (2016) 691–695. https://doi.org/10.1126/science.aad3345.

[2]   P. Simon, Y. Gogotsi, Materials for electrochemical capacitors, Nat. Mater. 7 (2008) 845–854. https://doi.org/10.1038/nmat2297.

[3]   P. Simon, Y. Gogotsi, Perspectives for electrochemical capacitors and related devices, Nat. Mater. 19 (2020) 1151–1163. https://doi.org/10.1038/s41563-020-0747-z.

[4]   C. Lethien, J. Le Bideau, T. Brousse, Challenges and prospects of 3D micro-supercapacitors for powering the internet of things, Energy Environ. Sci. 12 (2019) 96–115. https://doi.org/10.1039/C8EE02029A.

[5]   N.A. Kyeremateng, T. Brousse, D. Pech, Microsupercapacitors as miniaturized energy-storage components for on-chip electronics, Nat. Nanotechnol. 12 (2017) 7–15. https://doi.org/10.1038/nnano.2016.196.

[6]   B. Asbani, B. Bounor, K. Robert, C. Douard, L. Athouël, C. Lethien, J. Le Bideau, T. Brousse, Reflow Soldering-Resistant Solid-State 3D Micro-Supercapacitors Based on Ionogel Electrolyte for Powering the Internet of Things, J. Electrochem. Soc. 167 (2020) 100551. https://doi.org/10.1149/1945-7111/ab9ccc.

[7]   E. Eustache, C. Douard, A. Demortière, V. De Andrade, M. Brachet, J. Le Bideau, T. Brousse, C. Lethien, High Areal Energy 3D-Interdigitated Micro-

Supercapacitors in Aqueous and Ionic Liquid Electrolytes, Adv. Mater. Technol. 2 (2017) 1700126. https://doi.org/10.1002/admt.201700126.

[8] K. Robert, D. Stiévenard, D. Deresmes, C. Douard, A. Iadecola, D. Troadec, P. Simon, N. Nuns, M. Marinova, M. Huvé, P. Roussel, T. Brousse, C. Lethien, Novel insights into the charge storage mechanism in pseudocapacitive vanadium nitride thick films for high-performance on-chip micro-supercapacitors, Energy Environ. Sci. 13 (2020) 949–957. https://doi.org/10.1039/c9ee03787j.

[9] D.H. Alsem, N.J. Salmon, D.A. Shapiro, X. Liu, Y. Yu, W.C. Chueh, J. Lim, P. Bai, D.A. Cogswell, H. So, T. Tyliszczak, M.Z. Bazant, S.C. Lee, N. Jin, Y. Li, Origin and hysteresis of lithium compositional spatiodynamics within battery primary particles, Science (80-.). 353 (2016) 566–571. https://doi.org/10.1126/science.aaf4914.

[10] P. Zhang, Y. Li, G. Wang, F. Wang, S. Yang, F. Zhu, X. Zhuang, O.G. Schmidt, X. Feng, Zn-Ion Hybrid Micro-Supercapacitors with Ultrahigh Areal Energy Density and Long-Term Durability, Adv. Mater. 31 (2019) 1–6. https://doi.org/10.1002/adma.201806005.

[11] A. Balducci, D. Belanger, T. Brousse, J.W. Long, W. Sugimoto, Perspective—A Guideline for Reporting Performance Metrics with Electrochemical Capacitors: From Electrode Materials to Full Devices, J. Electrochem. Soc. 164 (2017) A1487–A1488. https://doi.org/10.1149/2.0851707jes.

[12] P. Simon, Y. Gogotsi, B. Dunn, Where Do Batteries End and Supercapacitors Begin?, Science (80-.). 343 (2014) 1210–1211. https://doi.org/10.1126/science.1249625.

[13]   Z. Zhao, X. Xu, G. Hao, H. Sun, Y. Huang, J. Liang, L. Mei, M. Li, C. Wang, C. Lee, I. Shakir, X. Duan, M. Ding, H. Fei, B. Dunn, J. Lau, B. Papandrea, Three-dimensional holey-graphene/niobia composite architectures for ultrahigh-rate energy storage, Science (80-.). 356 (2017) 599–604. https://doi.org/10.1126/science.aam5852.

[14]   M.R. Lukatskaya, S. Kota, Z. Lin, M.Q. Zhao, N. Shpigel, M.D. Levi, J. Halim, P.L. Taberna, M.W. Barsoum, P. Simon, Y. Gogotsi, Ultra-high-rate pseudocapacitive energy storage in two-dimensional transition metal carbides, Nat. Energy. 6 (2017) 1–6. https://doi.org/10.1038/nenergy.2017.105.

[15]   H.S. Kim, J.B. Cook, H. Lin, J.S. Ko, S.H. Tolbert, V. Ozolins, B. Dunn, Oxygen vacancies enhance pseudocapacitive charge storage properties of MoO3-x, Nat. Mater. 16 (2017) 454–462. https://doi.org/10.1038/NMAT4810.

[16]   V. Augustyn, J. Come, M.A. Lowe, J.W. Kim, P.-L. Taberna, S.H. Tolbert, H.D. Abruña, P. Simon, B. Dunn, High-rate electrochemical energy storage through Li+ intercalation pseudocapacitance, Nat. Mater. 12 (2013) 518–522. https://doi.org/10.1038/nmat3601.

[17]   E. Eustache, C. Douard, R. Retoux, C. Lethien, T. Brousse, MnO2 Thin Films on 3D Scaffold: Microsupercapacitor Electrodes Competing with "bulk" Carbon Electrodes, Adv. Energy Mater. 5 (2015) 3–7. https://doi.org/10.1002/aenm.201500680.

[18]   A. Ferris, S. Garbarino, D. Guay, D. Pech, 3D RuO2 Microsupercapacitors with Remarkable Areal Energy, Adv. Mater. 27 (2015) 6625–6629. https://doi.org/10.1002/adma.201503054.

[19]   A. Ferris, D. Bourrier, S. Garbarino, D. Guay, D. Pech, 3D Interdigitated

Microsupercapacitors with Record Areal Cell Capacitance, Small. 15 (2019) 1–8. https://doi.org/10.1002/smll.201901224.

[20]   J.W. Long, B. Dunn, D.R. Rolison, H.S. White, Three-dimensional battery architectures, Chem. Rev. 104 (2004) 4463–4492. https://doi.org/10.1021/cr020740l.

[21]   L. Baggetto, R.A.H. Niessen, F. Roozehoom, P.H.L. Notten, High energy density all-solid-state batteries: A challenging concept towards 3D integration, Adv. Funct. Mater. 18 (2008) 1057–1066. https://doi.org/10.1002/adfm.200701245.

[22]   M. Létiche, E. Eustache, J. Freixas, A. Demortière, V. De Andrade, L. Morgenroth, P. Tilmant, F. Vaurette, D. Troadec, P. Roussel, T. Brousse, C. Lethien, Atomic Layer Deposition of Functional Layers for on Chip 3D Li-Ion All Solid State Microbattery, Adv. Energy Mater. 7 (2017) 1–12. https://doi.org/10.1002/aenm.201601402.

[23]   Y. Lei, B. Daffos, P.L. Taberna, P. Simon, F. Favier, MnO2-coated Ni nanorods: Enhanced high rate behavior in pseudo-capacitive supercapacitor, Electrochim. Acta. 55 (2010) 7454–7459. https://doi.org/10.1016/j.electacta.2010.03.012.

[24]   J.P. Alper, S. Wang, F. Rossi, G. Salviati, N. Yiu, C. Carraro, R. Maboudian, Selective ultrathin carbon sheath on porous silicon nanowires: Materials for extremely high energy density planar micro-supercapacitors, Nano Lett. 14 (2014) 1843–1847. https://doi.org/10.1021/nl404609a.

[25]   T.M. Dinh, A. Achour, S. Vizireanu, G. Dinescu, L. Nistor, K. Armstrong, D. Guay, D. Pech, Hydrous RuO2/carbon nanowalls hierarchical structures for all-

solid-state ultrahigh-energy-density micro-supercapacitors, Nano Energy. 10 (2014) 288–294. https://doi.org/10.1016/j.nanoen.2014.10.003.

[26]   E. Eustache, P. Tilmant, L. Morgenroth, P. Roussel, G. Patriarche, D. Troadec, N. Rolland, T. Brousse, C. Lethien, Silicon-microtube scaffold decorated with anatase TiO2 as a negative electrode for a 3D litium-ion microbattery, Adv. Energy Mater. 4 (2014) 1–11. https://doi.org/10.1002/aenm.201301612.

[27]   S. Trasatti, G. Buzzanca, Ruthenium dioxide: A new interesting electrode material. Solid state structure and electrochemical behaviour, J. Electroanal. Chem. 29 (1971) 4–8. https://doi.org/10.1016/S0022-0728(71)80111-0.

[28]   S. Ardizzone, G. Fregonara, S. Trasatti, "Inner" and "outer" active surface of RuO2 electrodes, Electrochim. Acta. 35 (1990) 263–267. https://doi.org/10.1016/0013-4686(90)85068-X.

[29]   X. Wu, W. Xiong, Y. Chen, D. Lan, X. Pu, Y. Zeng, H. Gao, J. Chen, H. Tong, Z. Zhu, High-rate supercapacitor utilizing hydrous ruthenium dioxide nanotubes, J. Power Sources. 294 (2015) 88–93. https://doi.org/10.1016/j.jpowsour.2015.06.064.

[30]   B.E. Conway, Transition from "supercapacitor" to "battery" behavior in electrochemical energy storage, Proc. Int. Power Sources Symp. 138 (1991) 319–327. https://doi.org/10.1149/1.2085829.

[31]   J.P. Zheng, P.. Cygan, T.R. Jow, Hydrous Ruthenium Oxide as an Electrode Material for Electrochemical Capacitors, J. Electrochem. Soc. 142 (1995) 2699–2703. https://doi.org/10.1557/proc-393-433.

[32]   W. Sugimoto, H. Iwata, Y. Murakami, Y. Takasu, Electrochemical Capacitor

Behavior of Layered Ruthenic Acid Hydrate, J. Electrochem. Soc. 151 (2004) A1181. https://doi.org/10.1149/1.1765681.

[33] M.F. El-Kady, M. Ihns, M. Li, J.Y. Hwang, M.F. Mousavi, L. Chaney, A.T. Lech, R.B. Kaner, Engineering three-dimensional hybrid supercapacitors and microsupercapacitors for high-performance integrated energy storage, Proc. Natl. Acad. Sci. 112 (2015) 4233–4238. https://doi.org/10.1073/pnas.1420398112.

[34] S.G. Patnaik, J.S. Seenath, D. Bourrier, S. Prabhudev, D. Guay, D. Pech, Porous RuOxNySz Electrodes for Microsupercapacitors and Microbatteries with Enhanced Areal Performance, ACS Energy Lett. 6 (2021) 131–139. https://doi.org/10.1021/acsenergylett.0c02017.

[35] D. Gaboriau, M. Boniface, A. Valero, D. Aldakov, T. Brousse, P. Gentile, S. Sadki, Atomic Layer Deposition Alumina-Passivated Silicon Nanowires: Probing the Transition from Electrochemical Double-Layer Capacitor to Electrolytic Capacitor, ACS Appl. Mater. Interfaces. 9 (2017) 13761–13769. https://doi.org/10.1021/acsami.7b01574.

[36] M. Brachet, D. Gaboriau, P. Gentile, S. Fantini, G. Bidan, S. Sadki, T. Brousse, J. Le Bideau, Solder-reflow resistant solid-state micro-supercapacitors based on ionogels, J. Mater. Chem. A. 4 (2016) 11835–11843. https://doi.org/10.1039/c6ta03142k.

METHODS

Fabrication of the 3D scaffold. The manufacturing of 3D scaffold follows a technological process compatible with the microfabrication methods available in the semiconductor industry. Spin coating of a photoresist (SPR 220) is achieved on a (100) 3'' silicon wafer. A photolithography step is then applied to define the micro-tubes pattern following the process reported in[22,26]. The structure pitch, the outer and inner diameters of the micro-tubes pattern are 9 μm, 6 μm and 3 μm, respectively. The silicon wafer is micromachined to fabricate the silicon micro-tubes using the Bosch dry etching process. High aspect ratio silicon micro-tubes are then obtained and the etched depth is tuned with the number of Bosch cycles. From the geometric dimensions of the silicon micro-tubes scaffold, the area enhancement factor (AEF) of the template is calculated using the following formula (1): $AEF = 1 +$

$$\frac{(P_{IN} \times d_{IN} + P_{OUT} \times d_{OUT})}{pitch^2} \qquad (1)$$

where P_{IN} is the inner perimeter of the square shape silicon micro-tubes (4 x 3 μm), P_{OUT} is the outer perimeter of the micro-tubes (4 x 6 μm), d_{OUT} is the etched depth of the electrode and $d_{IN} = \frac{d_{OUT}}{2}$ (internal depth of the Si micro-tubes). The structure pitch (pitch parameter = 9 μm) corresponds to the sum of the spacing between micro-tubes and the outer diameter of the Si micro-tube.

Deposition of an insulator layer (Si_3N_4 or Al_2O_3) and a Pt current collector. The 3D micro-tubes scaffold was firstly covered with an insulator and protected layer to prevent damaging of the substrate. Depending on the selected deposition methods, either a thin layer of Si_3N_4 or Al_2O_3 was then deposited. Si_3N_4 (300 nm-thick) film was deposited by low-pressure chemical vapor deposition technique (LP CVD) at 800 °C (flow rates: 60 sccm for NH_3 and 20 sccm for SiH_2Cl_2) using a Tempress furnace

(deposition pressure = 100 mTorr). Alternatively, an Al_2O_3 film (100 nm-thick) could be deposited on the 3D silicon micro-tubes by Atomic Layer Deposition (ALD) method instead of the Si_3N_4 layer. Those layers acted as an insulator layer preventing the chemical etching of the silicon substrate by the aqueous electrolyte. The platinum current collector (50 nm-thick) was afterward deposited by ALD from a TFS200 Beneq ALD reactor; this technique ensured a conformal deposit on the 3D micro-tubes scaffold. Fifty 3D electrodes were reproducibly prepared on a single 3 inches silicon wafer. The reproducibility of the fabrication process and of the electrode performance were tested at least on 5 different electrodes from the same wafer. We report in this study the typical performance obtained on our RuO_2 electrodes.

Electrodeposition of hydrous RuO_2 films. The Si / Si_3N_4 / Pt (Si / Al_2O_3 / Pt) 3D current collector was then covered with a conformal RuO_2 pseudocapacitive film using electrodeposition method. The 3D Pt-current collector acted as the working electrode, while a Pt foil and an Ag/AgCl electrode were considered as the counter and reference electrodes, respectively. Cyclic voltammetry technique was applied between -0.3 and 1 V vs Ag/AgCl at 50 °C from a solution based on 5 mM $RuCl_3xH_2O$ in 10^{-1} M KCl / 10^{-2} M HCl. The number of electrodeposited cycles was tuned to reach the targeted thickness. An annealing step was achieved on 3D RuO_2 electrode at 150 °C during 1 h under air atmosphere to study the cycling stability.

Electrochemical characterizations. The electrochemical properties of RuO_2 electrodes were measured in a three-electrode configuration, in 0.5 M H_2SO_4 aqueous electrolyte. Here, the electrodeposited 3D RuO_2 electrodes were mounted in a Teflon homemade flat cell and were considered as the working electrode (WE). In this flat cell, a 3D electrode was get in sandwich between the two half-cells. The top

cell was holed and filled with the aqueous electrolyte in contact with the 3D RuO_2 electrode. An O-ring achieved the watertightness between the top cell and the sample under test. A platinum wire acted as the counter electrode and an Ag/AgCl reference electrode was used to monitor the potential during the electrochemical analyses. Cyclic voltammetry (CV) and electrochemical impedance spectroscopy (EIS) were carried out on a Biologic VMP3 potentiostat/galvanostat equipment. The cycling stability of two 3D RuO_2 electrodes was evaluated in 0.5 M H_2SO_4 aqueous electrolyte. The as-deposited 3D RuO_2 electrode was cycled at 50 mVs^{-1} between 0 and 0.9 V vs Ag/AgCl while the air-annealed 3D RuO_2 electrode was tested at 25 mVs^{-1} between 0.1 and 0.9 V vs Ag/AgCl. The initial capacitance value of the as-deposited sample and annealed one at 150 °C were similar. Consequently, for classical electrochemical characterization (cyclic voltammetry and electrochemical impedance spectroscopy measurement), all the samples were not annealed at 150 °C. Unfortunately, it was not possible to obtain a good cycling stability without an annealing step. Consequently, only the sample used for long-term cycling experiments was annealed at 150 °C after the electrodeposition process of ruthenium dioxide film.

Structural and morphological characterizations. A Zeiss Ultra 55 scanning electron microscope (SEM) was used to determine the morphology (cross section and top view analyses) of the 3D scaffold and the deposited RuO_2 films. A Raman spectrometer with a 471 nm UV laser source was used to study the film structure. TEM measurements were conducted on a S/TEM FEI TITAN Themis 300 equipped with a probe corrector for a resolution of 0.6 Å in STEM mode, a Super-X quad EDS detector for elemental analysis. The TEM samples (~150 nm-thick) were prepared using the Focused Ion Beam (FIB) technique (FEI Strata Dual Beam 235 equipment).

One 3D micro-tube coated with the stacked layer was isolated from the substrate and was laid down horizontally on a silicon wafer. A platinum layer was deposited on the top of the horizontal micro-tube in order to protect the samples from the FIB preparation.

LIST OF THE FIGURES AND FIGURE CAPTIONS
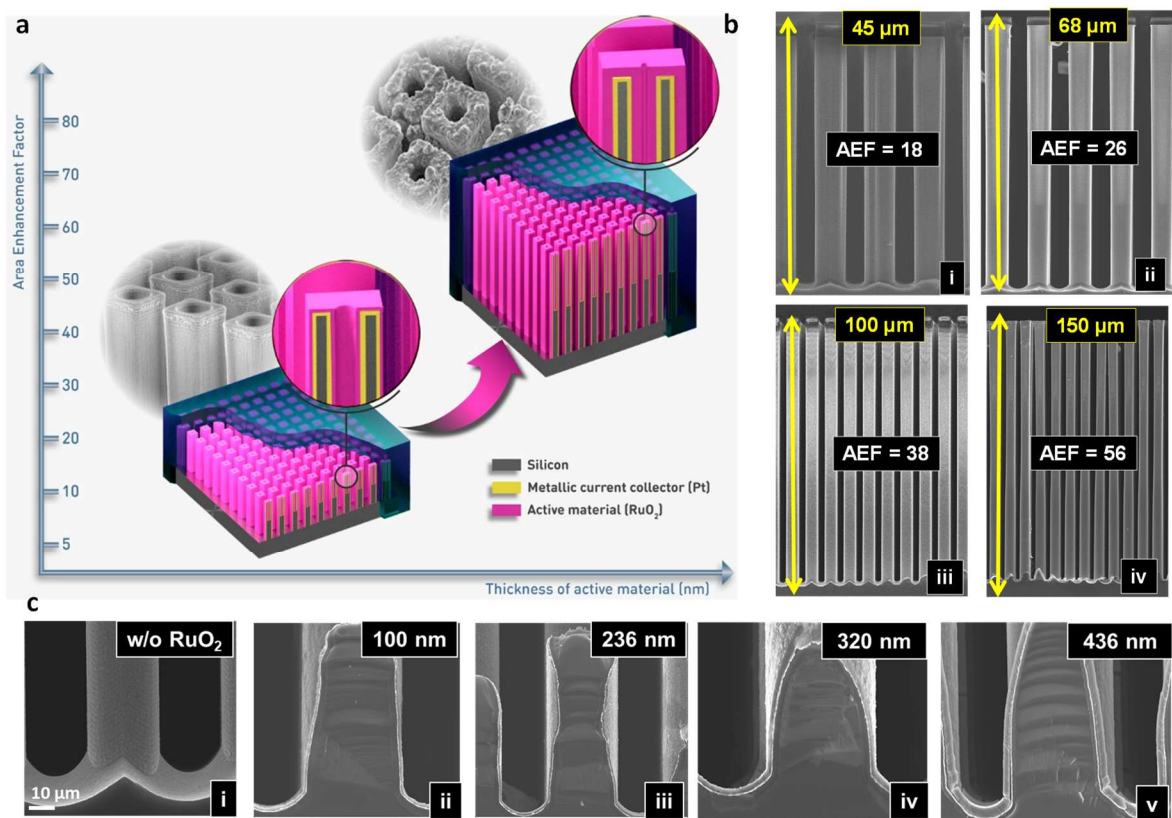
Fig. 1 | a. Proposed strategies used to improve the areal capacitance values of an electrode by tuning both the Area Enhancement Factor (AEF) and the thickness of active material**. b.** SEM cross-section imaging of 3D silicon micro-tubes with different etched depths. **c.** SEM cross-section analyses of 3D Si micro-tubes (100 µm-depth) coated with RuO_2 films with different thicknesses from 100 to 436 nm.
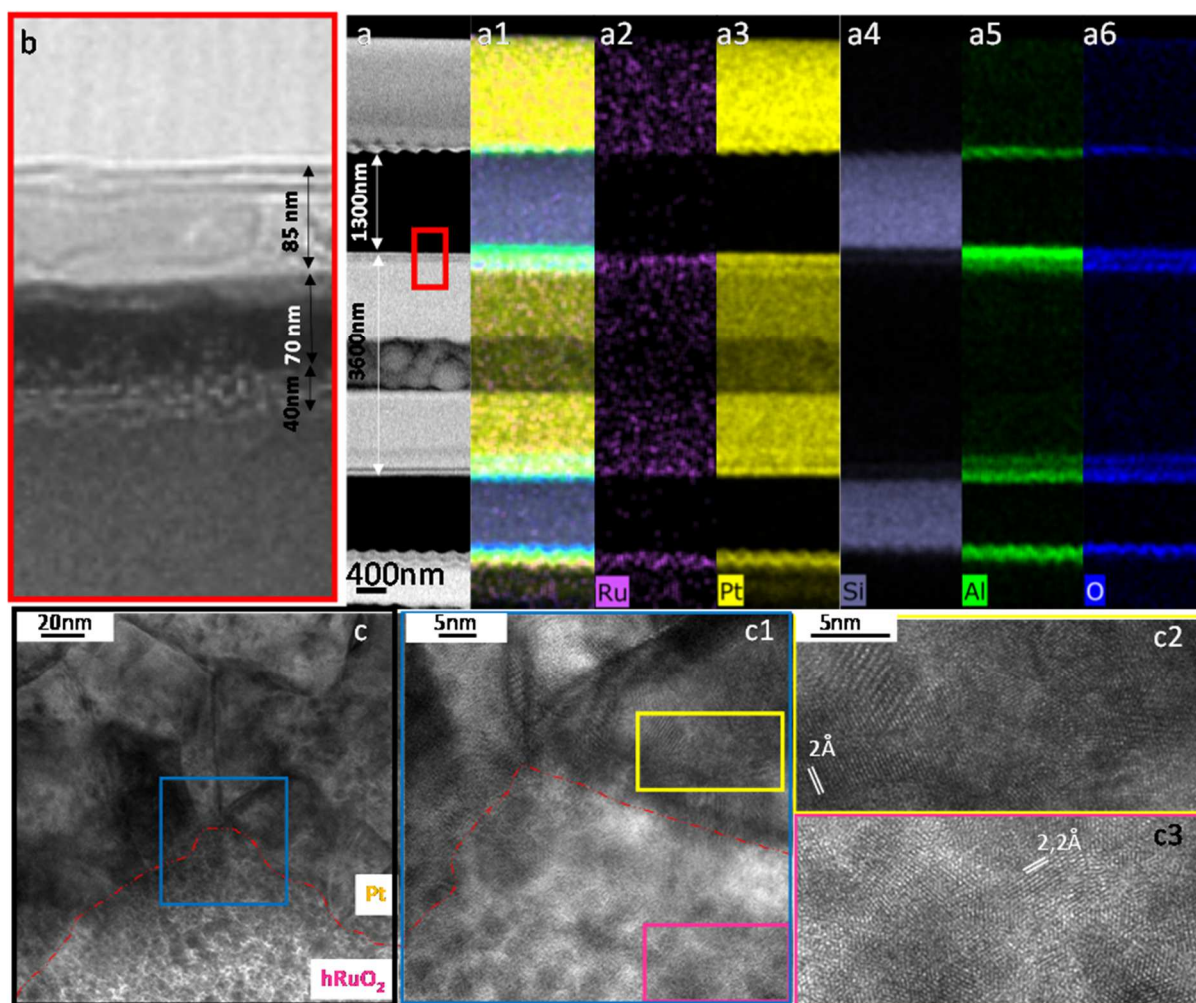
Fig. 2 | S)TEM and EDS analyses. a. HAADF image showing a cross section of the 3D electrode and the corresponding EDS mapping of the different elements (from a_1 to a_6 panels). **b.** TEM image corresponding to the red area of the image a. **c.** Enlargement of the black zone of the b-image showing the interface between Pt and $hRuO_2$ layers. The red line indicates the interface between a Pt grain and $hRuO_2$ grain as confirmed by the large difference in the contrast. **c1**. Zoom of the blue area of image d. **c2 and c3**. Zoom of the yellow and pink areas of image d1. The RuO_2 phase as well as the Pt grain present fringes indicative of crystallized nanodomains.
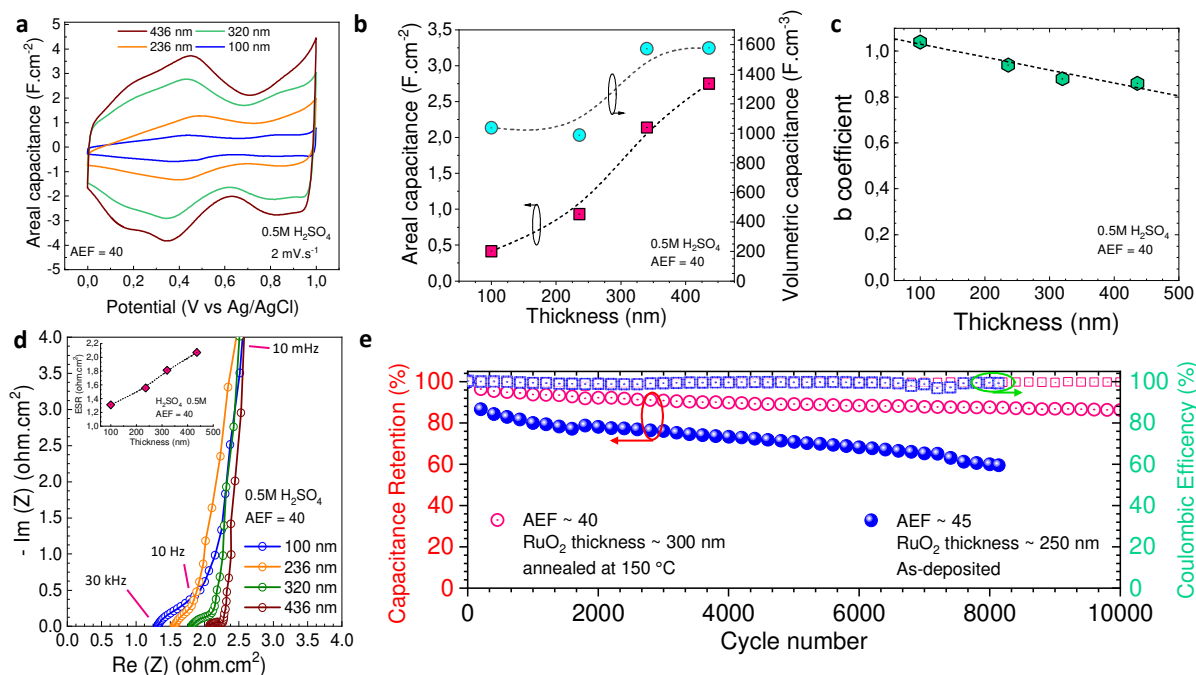
Fig. 3 | Electrochemical performance of the 3D RuO₂ electrodes in 0.5 M H₂SO₄ aqueous electrolyte with various thicknesses taking constant the AEF of the 3D scaffold (AEF = 40). a. CV at 2 mVs^{-1} vs the thickness of the RuO₂ films. **b.** Evolution of the areal and volumetric capacitances determined from CVs at 2 mVs^{-1} with increasing RuO₂ thickness from 100 to 436 nm. **c.** b-coefficient from $I_{peak} = av^b$ relationship vs the film thickness. **d.** Nyquist plots of the 3D RuO₂ electrodes with various thicknesses. The inset shows the evolution of the equivalent series resistance (ESR) with the RuO₂ thickness. **e.** Capacitance retention of two 3D RuO₂ electrodes (as deposited and air-annealed at 150 °C during 1h) and coulombic efficiency vs the number of cycles.
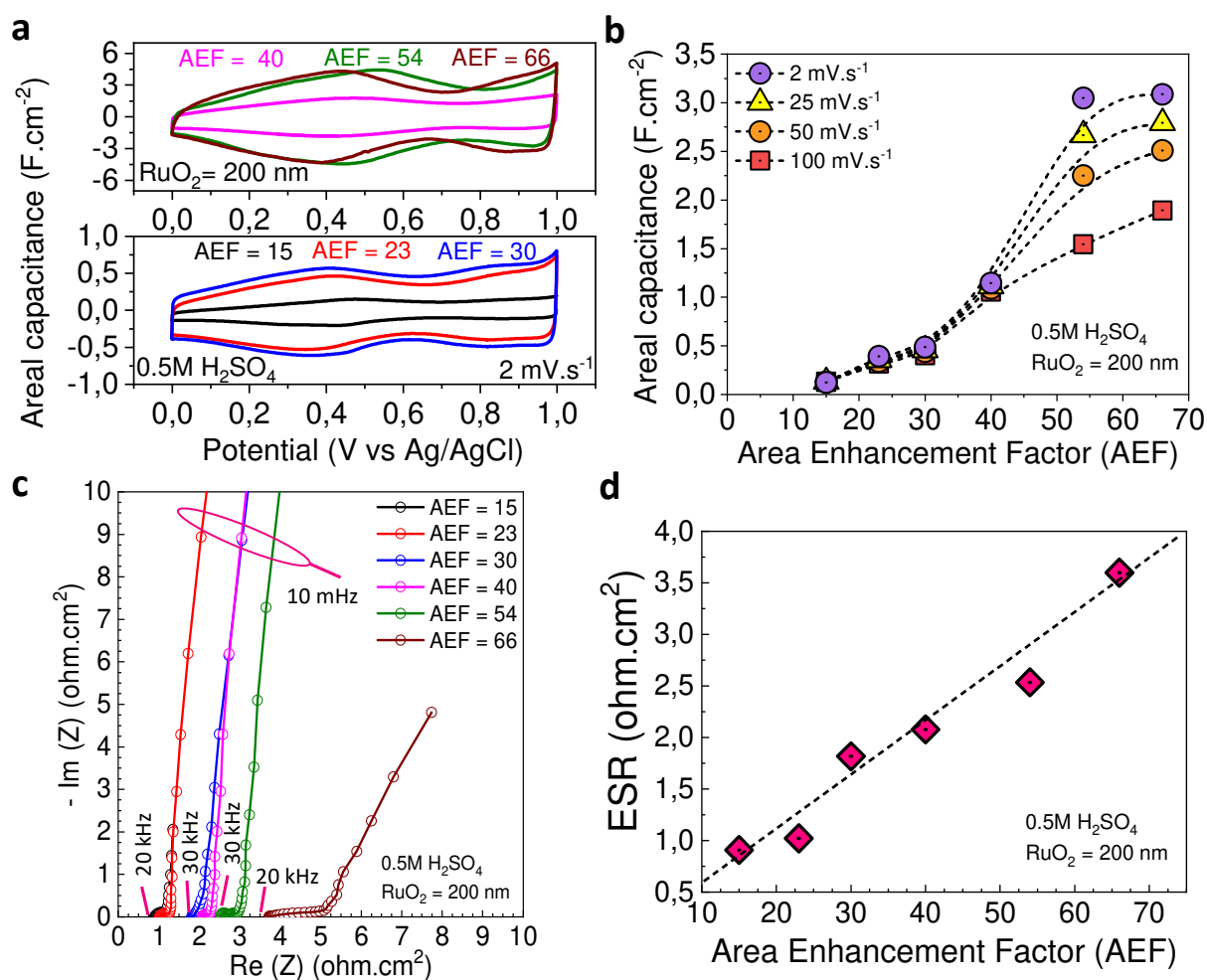
Fig. 4 | Electrochemical performance of the 3D RuO₂ electrode in 0.5 M H₂SO₄ depending on the AEF of the 3D scaffold (using a constant film thickness ~200 nm). a. Three electrode CV plots at 2 mVs⁻¹ of various 3D RuO₂ electrodes showing different area enhancement factor (AEF value between 15 and 66). **b.** Areal capacitance of 3D RuO₂ electrodes versus the sweep rates from 2 to 100 mVs⁻¹. **c.** Impedance spectra measured for different AEF values in 0.5 M H₂SO₄ at open circuit voltage. **d.** Variation of the equivalent series resistance (ESR) *vs* the AEF.

a

b
200 nm
427 nm
AEF 66
2 mV.s⁻¹
0.5M H₂SO₄
Areal capacitance (F.cm⁻²)
Potential (V vs Ag/AgCl)

c
AEF 66
RuO₂ = 427 nm
RuO₂ = 200 nm
0.5M H₂SO₄
Charge, q* (C.cm⁻²)
Scan rate (mV.s⁻¹)

d
AEF 66
RuO₂ = 427 nm
RuO₂ = 200 nm
0.5M H₂SO₄
Charge, q* (C.cm⁻²)
Scan rate⁻⁰·⁵, mV⁻⁰·⁵.s⁰·⁵

e
AEF 66
RuO₂ = 427 nm
RuO₂ = 200 nm
0.5M H₂SO₄
Charge⁻¹, 1/q* (C⁻¹.cm²)
Scan rate⁰·⁵, (mV.s⁻¹)⁰·⁵

f
q from outer surface
q from CV @ 2mV.s⁻¹
q total
Charge (C.cm⁻²)
1,5   3   3,125   1,75   4,2   5
200   427
RuO₂ thickness on 3D (AEF = 66)

g
Areal capacitance (F.cm⁻²)
High capacitance & high rate capabilities
This work
[16]
[15]
[13]
[14]
[9, 11]
[5-6]
[9]
[10]
[12]
[7-8]
[1]
[2]
[3]
[4]
High capacitance & low rate capabilties
Thickness of active material (μm)

[1] Nano Lett., 2014, 14, 1843–1847.
[2] Chem. Commun. 2013 , 49 , 4456 .
[3] Adv. Funct. Mater., 2016, 26, 1830–1839
[4] J. Power Sources, 2012, 197, 325–329.
[5] Energy Environ. Sci., 2014, 7, 2652–2659.
[6] Nano Energy, 2014, 10, 288–294.
[7] Adv. Energy Mater., 2015, 5, 3–7.
[8] Adv. Mater. Technol., 2017, 1700126.
[9] Energy Storage Mat 2021, 36, 520-527

[10] J. Power Sources, 2013, 221, 228–231.
[11] Proc. Natl. Acad. Sci., 2015, 112, 4233–4238.
[12] Electrochim. Acta, 2011, 56, 9508–9514.

[13] Adv. Mater., 2015, 27, 6625–6629.
[14] ACS Appl. Mater. Interfaces, 2016, 8, 13458–13465.
[15] Small 2019, 1901224
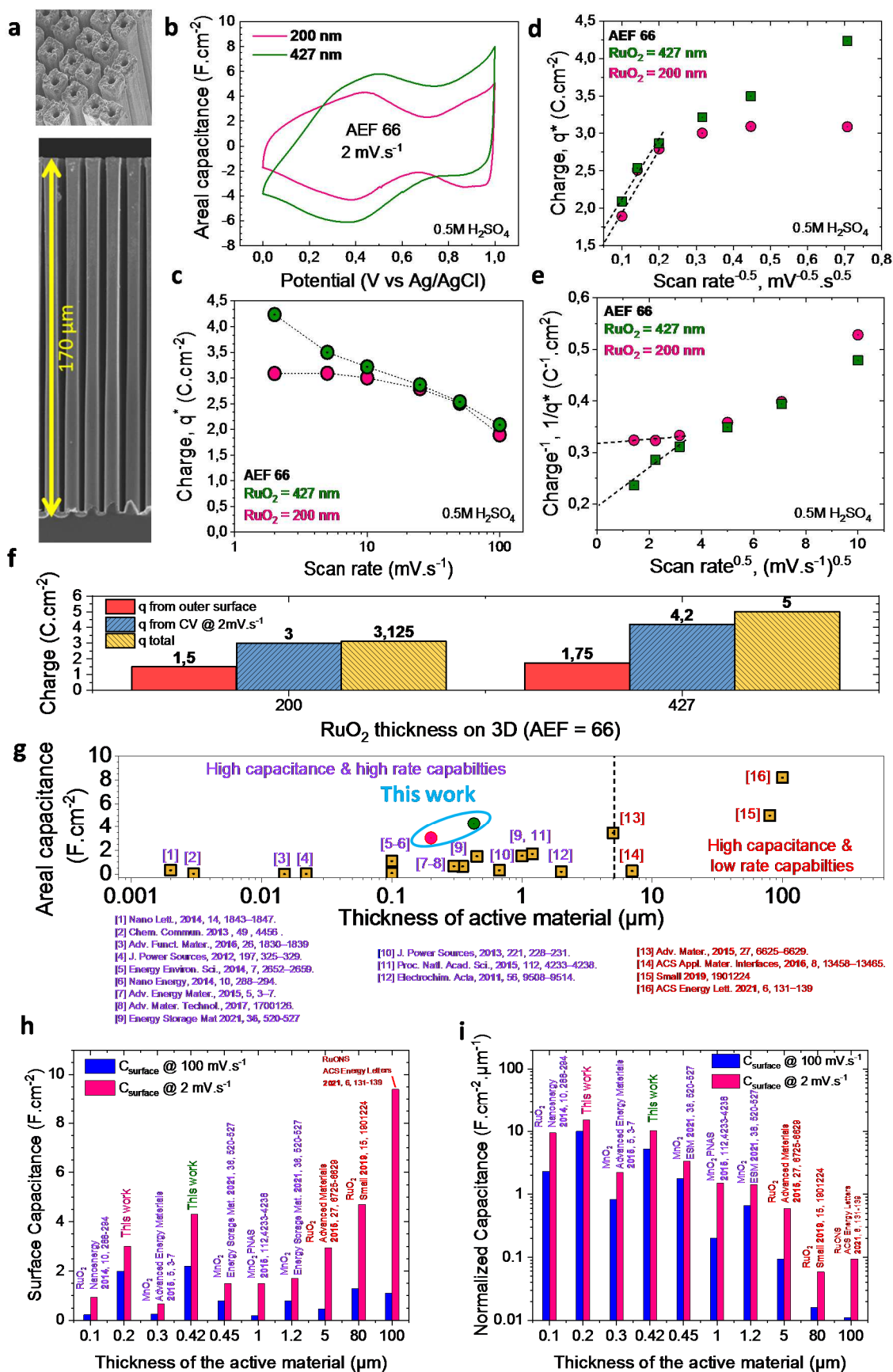[16] ACS Energy Lett. 2021, 6, 131–139

h
C_surface @ 100 mV.s⁻¹
C_surface @ 2 mV.s⁻¹
RuONS ACS Energy Letters 2021, 6, 131–139
Surface Capacitance (F.cm⁻²)
RuO₂ Nanoenergy 2014, 10, 288-294
This work
MnO₂ Advanced Energy Materiala 2015, 5, 3-7
This work
MnO₂ Energy Storage Mat. 2021, 36, 520-527
MnO₂ PNAS 2015, 112, 4233-4238
MnO₂ Energy Storage Mat. 2021, 36, 520-527
RuO₂ Advanced Materials 2015, 27, 6725-6629
RuO₂ Small 2019, 15, 1901224
Thickness of the active material (μm)

i
C_surface @ 100 mV.s⁻¹
C_surface @ 2 mV.s⁻¹
Normalized Capacitance (F.cm⁻².μm⁻¹)
RuO₂ Nanoenergy 2014, 10, 288-294.
This work
MnO₂ Advanced Energy Materiale 2015, 5, 3-7
This work
MnO₂ Energy Storage Mat. 2021, 36, 520-527
MnO₂ PNAS 2015, 112, 4233-4238
MnO₂ ESM 2021, 36, 520-527
RuO₂ Advanced Materials 2015, 27, 6725-6629
RuO₂ Small 2019, 15, 1901224
RuONS ACS Energy Letters 2021, 6, 131-139
Thickness of the active material (μm)

Fig. 5 | Benchmarking of the ultra-high areal capacitance 3D RuO$_2$ electrode. a. SEM images of the 170 µm-depth 3D scaffold (AEF = 66). **b.** CVs of the high areal capacitance electrodes (AEF = 66 / RuO$_2$ thickness = 200 and 427 nm respectively) at 2 mVs^{-1} in 0.5 M H$_2$SO$_4$ aqueous electrolyte. **c.** Areal rate performance of 3D electrodes (AEF = 66 / RuO$_2$ thickness = 200 & 427 nm respectively). **d.** Evolution of the charge, q*, versus 1/(sweep rate)$^{0.5}$. **e.** Evolution of inverse charge, 1/q*, versus square root of sweep rate. **f.** Determination of the charge contribution (q$_{outer\_surface}$, q$_{total}$, q measured from CV at 2 mVs^{-1}.) versus the thickness using a constant AEF (AEF = 66). **g.** Benchmark of the electrodes prepared in the present study regarding the existing 3D electrodes for 3D MSCs. **h-i.** Benchmarking of the proposed technology: this plot reports the evolution of the areal capacitance measured at 2 and 100 mVs^{-1} versus the thickness of the active material used to fabricate electrode for micro-supercapacitors. The performance of two 3D RuO$_2$ electrodes (electrode 1: AEF = 66, RuO$_2$ = 200 nm / electrode 2: AEF = 66, RuO$_2$ = 427 nm) fabricated in the present study are compared with previously reported high performance 3D electrodes.